Angular distribution of the bremsstrahlung emission during lower hybrid current drive on PLT

ANGULAR DISTRIBUTION OF THE BREMSSTRAHLUNG EMISSION DURING LOWER HYBRID CURRENT DRIVE ON PLT

S. VON GOELER, J. STEVENS, S. BERNABEI,
M. BITTER, T.K. CHU, P. EFTHIMION, N. FISCH,
W. HOOKE, K. HILL, J. HOSEA, F. JOBES,
C. KARNEY, J. MERVINE, E. MESERVEY,
R. MOTLEY, P. RONEY, S. SESNIC,
K. SILBER, G. TAYLOR
Princeton Plasma Physics Laboratory,
Princeton University,
Princeton, New Jersey,
United States of America

ABSTRACT. The bremsstrahlung emission from the PLT tokamak during lower-hybrid current drive has been measured as a function of angle between the magnetic field and the emission direction. The emission is peaked strongly in the forward direction, indicating a strong anisotropy of the electron velocity distribution. The data demonstrate the existence of a nearly flat tail of the velocity distribution, which extends out to approximately 500 keV and which is interpreted as the plateau created by Landau damping of the lower-hybrid waves.

1. INTRODUCTION

Hard-X-ray spectra recorded during 800 MHz lower-hybrid current drive on the Princeton Large Torus (PLT) tokamak have shown that a non-Maxwellian tail of energetic electrons is formed by the RF waves [1]. The electron tail is thought to be formed by Landau damping of the lower-hybrid waves. To gain an understanding of the physics of lower-hybrid current drive, it is necessary (a) to investigate the propagation of the lower-hybrid waves in the plasma, and (b) to study the evolution of the electron velocity distribution. This paper addresses the second point. It presents measurements of the shape of the electron velocity distribution during lower-hybrid current drive.

A good opportunity to obtain information on the velocity distribution function of energetic electrons is provided by the bremsstrahlung produced in collisions between electrons and ions. In particular, the forward scattering of bremsstrahlung for relativistic electrons can be used to investigate the anisotropy of the distribution function, which is crucial for estimating the efficiency of the current drive. Therefore, an experiment has been carried out on the PLT tokamak to measure the angular distribution of the hard-X-ray emission, i.e. the dependence of the X-ray intensity on the angle θ between the emission direction and the toroidal magnetic field of the tokamak. Because of the scarcity of

tangential ports on PLT, our equipment was installed on the machine for a relatively short time period only, from November 1982 to February 1983. In this paper we present the results of this experiment; in an accompanying paper [2] we describe the modelling of the bremsstrahlung spectra. Preliminary results have been reported already at the Madison conference on RF heating [3].

The paper is divided as follows: a brief description of the experimental apparatus is given in Section 2. The details of the data-taking and evaluation procedure for a typical lower-hybrid discharge with 90° phasing of the waveguide grill are described in Section 3. Radial profile measurements of the hard-X-ray emission are presented in Section 4. The available information on the dependence of the distribution function on parameters and discharge conditions is reported in Section 5.

2. EXPERIMENTAL APPARATUS

The experiment is based on the forward scattering of X-ray bremsstrahlung for relativistic electrons, which is illustrated in Fig.1. In the graph, X-ray emission cones are plotted for electrons of 20, 50, 100, 200 and 500 keV energy. The electrons are assumed to go from left to right, and the distance from the
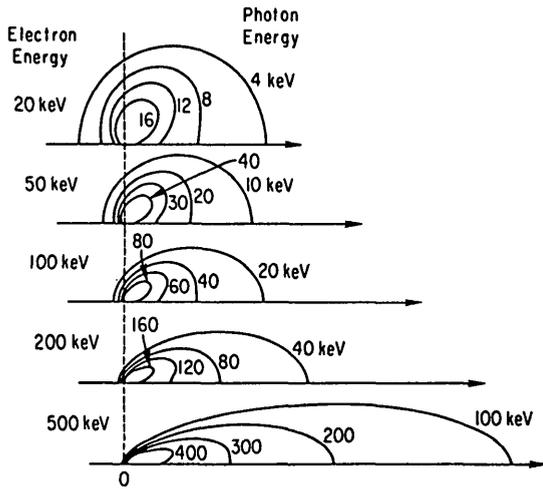
FIG.1. Bremsstrahlung emission cones for mildly relativistic electrons.
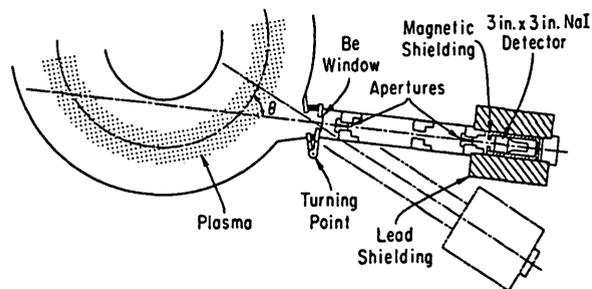
FIG.2. Schematic of tangential hard-X-ray detector on PLT.

origin to one of the curves is proportional to the emitted radiation power per steradian per photon-energy interval. An electron with kinetic energy E emits X-ray photons which have energies $h\nu$ smaller than E. For a 20 keV electron, for example, we plot the 16, 12, 8 and 4 keV emission cones. The X-ray emission consists predominantly of electron-ion bremsstrahlung. A detailed discussion of the formulas that are used, as well as of the contributions that result from electron-electron bremsstrahlung and recombination radiation, is given in the accompanying paper [2]. For relativistic electrons with an energy of 500 keV, the emission is pointed strongly in the forward direction. However, even for 20 keV electrons, the major part of the emission is in the forward direction, although the cone is not very narrow. For energetic electrons with speed primarily along the magnetic field lines, we

expect the X-ray emission to be strongly peaked in the direction of the toroidal field and opposite to the direction of the plasma current. The same measurement principle has been utilized previously for different purposes on mirror machines [4] and on tokamaks [5].

The experimental apparatus to measure the X-ray emission cones, the 'Tangential Detector', is sketched in Fig.2. A 3 in. X 3 in. sodium-iodide detector views the plasma midplane through a series of lead apertures at an angle θ with respect to the magnetic axis of the plasma. To change the angle θ, the whole apparatus is tilted around a turning point on the vacuum vessel. In the experimental setup that was used on PLT, the detector could be moved from an angle $\theta = 86°$ to an angle $\theta = 28°$.

A 3 in. X 3 in. NaI detector was chosen because of its large photo-peak-detection efficiency. For large photon energies, the cross-section for Compton scattering dominates, and photons are scattered out of the crystal before they deposit their full energy. A large scintillator improves the photo-peak efficiency because it captures the scattered photons. The photo-peak efficiency and the absorption efficiency for a centrally illuminated 3 in. X 3 in. NaI crystal are plotted in Fig.3. For an allowed maximum error of 50%, inconvenient unfolding of spectra and efficiency corrections can be avoided with the 3 in. X 3 in. detector if the spectra do not extend beyond $h\nu = 850$ keV. A 4 in. lead wall shields the detector all around against the hard-X-ray background radiation. The amount of background radiation can be easily determined by plugging the front aperture. It was necessary to add another 8 in. of lead shielding in the direction of the limiter in order to suppress hard X-rays. During the 800 MHz lower-hybrid current drive, neutrons did not present a problem. However, for slightly higher densities ($\bar{n}_e > 1 \times 10^{13}$ cm^{-3}), when the neutron yield exceeded 10^9 neutrons per second, there was a noticeable background that originated from n-γ reactions.
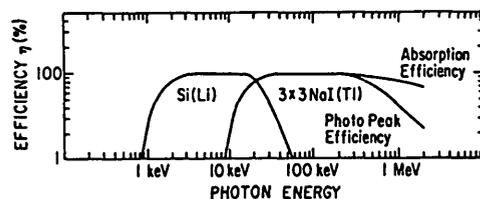
FIG.3. Photo peak and absorption efficiency for lithium-drifted silicon Si(Li) and for 3 in. X 3 in. sodium iodide NaI (Tl) detectors used for PLT experiments.

Another potential problem is caused by hard-X-ray radiation which is emitted from the vacuum vessel walls. With the tangential detector, it was impossible to rule out the presence of wall radiation. However, we had available another hard-X-ray detector, which was installed underneath the machine (Fig.4) and whose line of sight at both entrance and exit included only beryllium windows that were recessed a distance of 1.5 feet from the vacuum vessel back into the wedge casting of the torque frame. This instrument is believed to be free from wall radiation since it has been carefully aligned so that the detector looks only at the recessed Be-windows and not at the wall. The spectra measured with this detector were identical to the spectra measured with the tangential detector at the position $\theta = 86°$. When the tangential detector was moved to other angles, there were no protrusions of the vacuum vessel wall or other obstacles which might have acted as a source of wall radiation. Other evidence that our spectra consist of plasma radiation and not wall radiation came from impurity injection. During molybdenum injection, the X-ray intensity increased by a factor of about three and decayed with a time constant of 30 to 50 ms. The enhanced X-ray emission is believed to be due to a Z_{eff} increase and reflects typical behaviour for impurity-ion confinement. The vertical detector fulfilled an additional purpose as a monitor to check
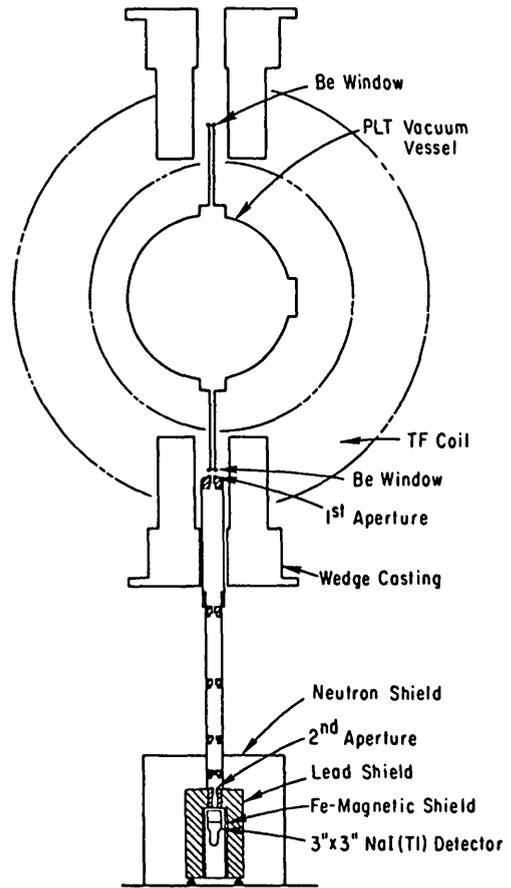
FIG.4. Schematic of vertical hard-X-ray detector on PLT.
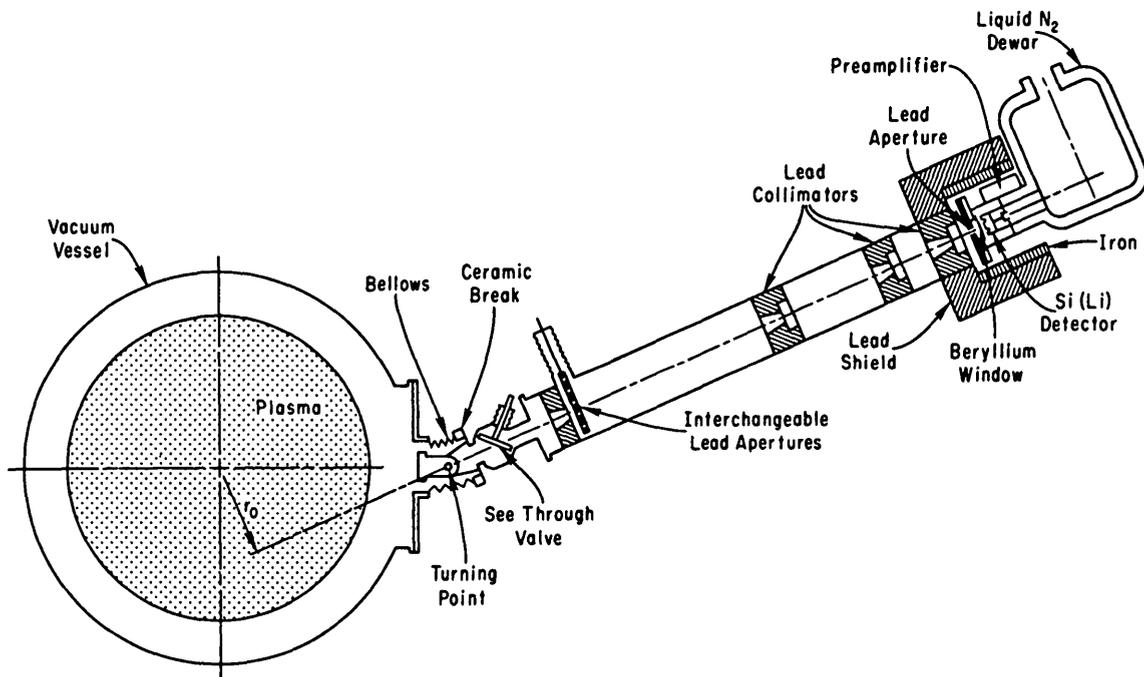
FIG.5. Schematic of soft-X-ray PHA system used to obtain radial profiles of hard-X-ray emission on PLT.
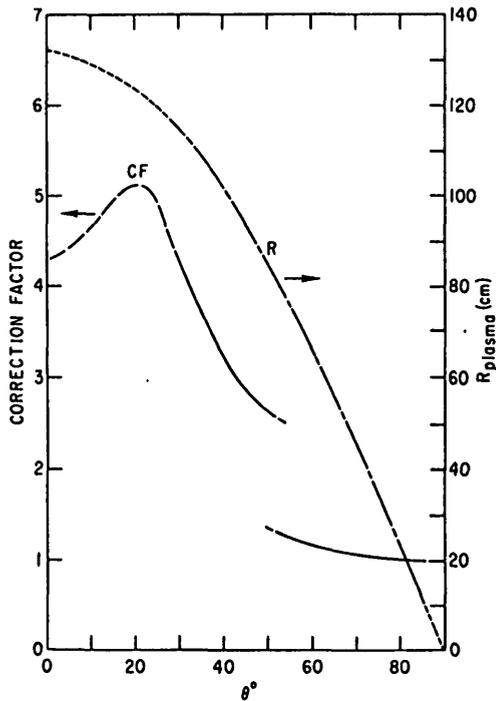
FIG.6. *Typical geometry-correction factor (CF) for tangential detector viewing plasma along chord tangential to circle with major radius R at angle θ with respect to PLT magnetic axis. Exact shape of correction factor depends on radial emission profile. Curve presented here is based on radial profile shown in Fig.10.*

the intensity of the electron tail at a photon energy of 14 keV have been used to calculate chord-length correction factors for the tangential detector. A typical example for such a chord-length correction is plotted in Fig.6 versus tangential viewing angle θ. Also shown is the plasma major radius at chord tangency. The largest tangent major radius accessible was 117 cm, whereas the PLT tokamak has a major radius of 132 cm.

To obtain measurements of the X-ray emission in the backward direction, the plasma current, the magnetic field, and the phasing of the RF waveguide grill are reversed. Unfortunately, the current-drive efficiency frequently is not exactly the same for the reversed discharges. Under these circumstances, instead of going through the extensive period of operation required to optimize the reversed discharges, the power level of the RF was adjusted so that the derivative of the plasma current vanishes ($\dot{I} = 0$). Also, the X-ray intensity is multiplied by a normalizing factor, which is obtained by comparing the spectra from the vertical detector before and after the current reversal.

3. ELECTRON VELOCITY DISTRIBUTION DURING A TYPICAL DISCHARGE WITH LOWER-HYBRID CURRENT DRIVE

In this section we present the details of the analysis of a typical lower-hybrid current-drive case with the 800 MHz RF system.

whether the hard-X-ray emission stayed constant from shot to shot during a θ-scan by the tangential detector.

During a θ-scan by the tangential detector, the chord length of the observed plasma changes. Actually, the detector looks twice through the plasma for angles θ smaller than 52°, as is readily evident from Fig.2. The weighted chord length in the plasma does depend on the radial profile of the plasma emission, and a θ-scan, consequently, must be combined with a radial profile measurement. During the time when the tangential detector was in operation on the machine, the only possible way to obtain information on the radial distribution was to measure profiles with the X-ray pulse height analyser (PHA) system, which is equipped with lithium-drifted silicon detectors (Fig.5). The X-ray PHA system normally measures the thermal part of the X-ray spectrum. However, the energetic electrons produced during LH current drive also show up on the PHA spectra as a non-Maxwellian tail. Because of the small size of the Si(Li) crystal, the more energetic photons go right through the detector without interacting, and the detector efficiency becomes very small for photon energies larger than 25 keV. Radial profiles of

FIG.7. *Plasma conditions for lower-hybrid current-drive discharge discussed in Section 3. Plotted are plasma current I_p, line-average electron density $\bar{n}_e$ from microwave interferometer, plasma loop voltage V_L, Shafranov parameter $\beta_\theta + \ell_i/2$, and RF power versus time. (a) plasma current in normal direction; (b) plasma current in reverse direction.*

The discharge conditions are shown in Fig.7a, where we plot the plasma current I_p, the line-average electron density $\bar{n}_e$, the Shafranov parameter $\beta_\theta + \ell_i/2$ from the equilibrium field, the loop voltage V_L, and the RF power P_{rf} versus time. Figure 7b gives the same quantities for the reversed discharge. The phasing of the waveguides was $-90°$ for Fig.7a and $+90°$ for Fig.7b. The RF was switched on at time $t = 100$ ms. There is a small increase in current from time 100 to 200 ms because a residual Ohmic voltage remains during that time. After time $t = 200$ ms the plasma current stays constant until time $t = 500$ ms. Although the RF power was considerably higher for the reversed current and although the plasma density was lower, the RF power could not quite keep the current up in the reversed discharge.

X-ray spectra collected during the time interval 250 ms $< t < 500$ ms are shown in Fig.8 and in Figs 9a and b. The raw data are displayed in Fig.8. The dots represent the photon count in a 3 keV energy band summed over five discharges. The data are measured at an angle $\theta = 28°$ between the magnetic axis and the line of sight. The data points are fitted by a curve which consists of the sum of two exponential functions
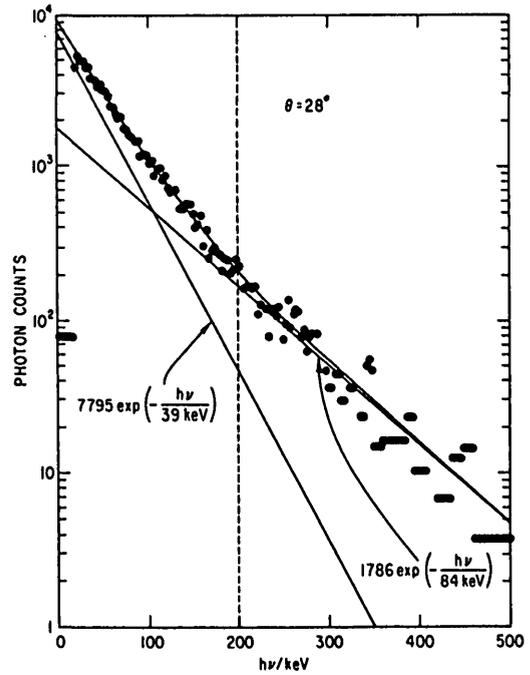
FIG.8. Hard-X-ray spectrum measured at angle $\theta = 28°$ in forward direction. Experimental points are fitted by 'two-temperature fit', a curve consisting of sum of two exponential functions.
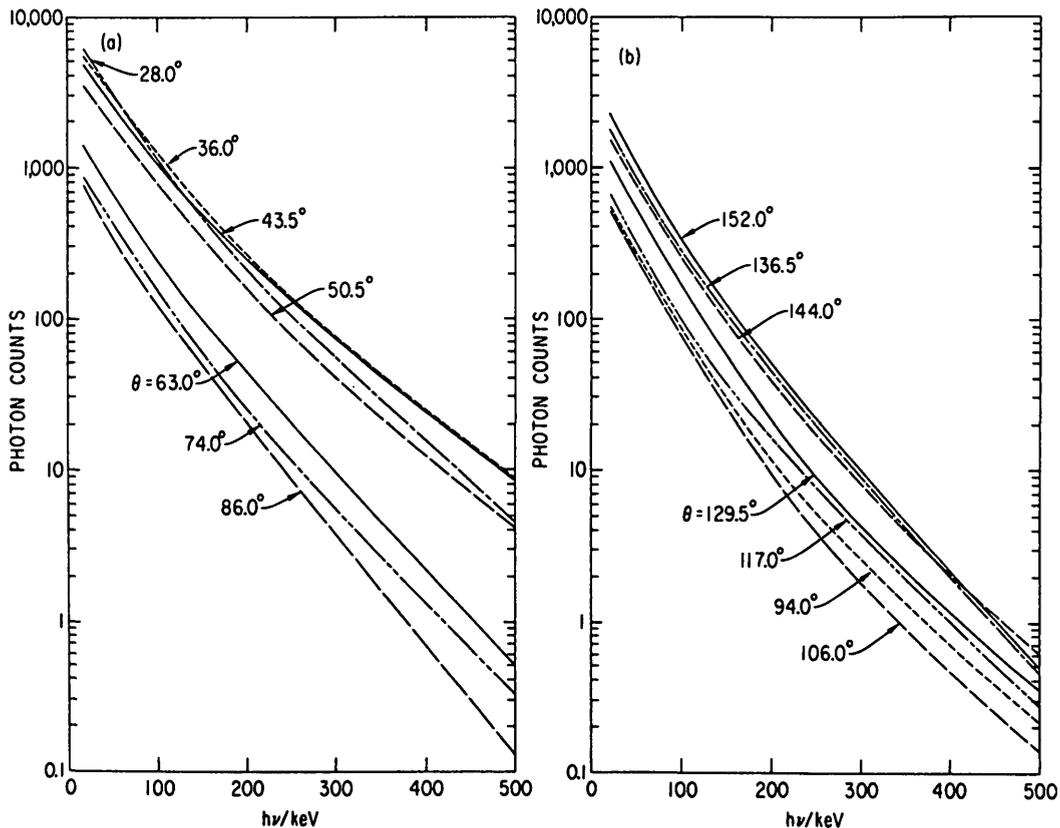
FIG.9. Fitted spectra with detector angle θ as parameter for normal discharge (a) and for reversed discharge (b). No geometry correction has been applied yet.
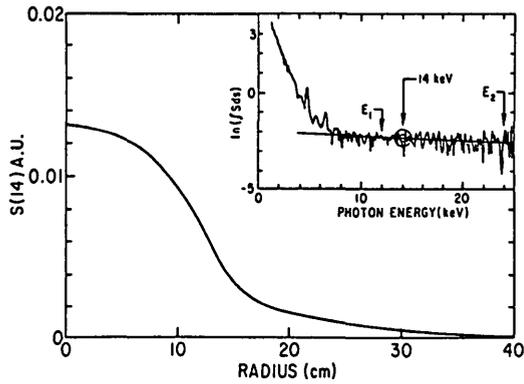
FIG.10. Abel-inverted radial profile of X-ray intensity at
hν = 14 keV photon energy obtained with soft-X-ray PHA system.
Insert shows typical soft-X-ray spectrum. Tail is fitted between
energy E_1 and E_2 by straight line in order to obtain X-ray
emission at photon energy of 14 keV.

and is called 'two-temperature fit'. The fitting proce-
dure is an iteration: First, an exponential function is
fitted to the data in the region hν $\leqslant$ 200 keV by least
squares. In the region hν > 200 keV, the exponential
function is subtracted from the data, and a second
exponential function is fitted to the difference. This
procedure is repeated for several cycles. In Figs 9a and b,
we plot the fitted curves with the angle θ as parameter
for the normal and the reversed discharge, respectively.
The vertical detector (Fig.4), which is used to monitor
the X-ray emission, showed a slightly smaller X-ray
intensity during the reversed discharges. Therefore, all
the data in Fig.9b have been multiplied with a normal-
ization factor 1.2. The curves shown in Fig.9 are not
corrected for geometrical efficiency. Therefore, a con-
siderable fraction of the variation of the X-ray intensity
with angle θ is due to variations of the effective chord
length. To correct for chord length, a radial profile
of the X-ray tail has been measured with the Si(Li)
detector (Fig.10). To obtain this curve, a straight line
was fitted through the measured X-ray spectrum in the
tail region, in the range from hν = 12 keV to 25 keV
(see inset Fig.10). The chord intensity at hν = 14 keV
is Abel-inverted and the result is labelled S(14). The
error for the radial profile is estimated to be 20 to 30%
and is due mostly to the inaccuracies associated with
the Abel inversion. At radii larger than 20 cm, the
X-ray intensity is very low and becomes comparable to
wall radiation [6]. Therefore, the intensity in the wing
of the profile is, possibly, somewhat overestimated.
The correction factor for the tangential detector which
results from these data is shown in Fig.6, and was dis-
cussed in Section 2.

Our final result, the X-ray intensity as a function of
angle θ for photon energies hν = 100 keV, 200 keV,
300 keV, and 400 keV is shown in Fig.11. The X-ray
emission seems to be nearly isotropic in the backward
direction. The emission increases strongly in the
forward direction. The increase amounts to a factor
of four for photon energies around 100 keV and to a
factor of 10 for photon energies around 400 keV.

To interpret the data shown in Fig.11, we have
developed a computer code that calculates the X-ray
bremsstrahlung emission produced by a hypothetical
electron distribution. The details of these modelling
calculations, as well as the error limits and uncertainties
that are associated with the modelling, are described in
detail in the accompanying paper [2]. Here, we only
want to summarize the main physics results that are
obtained from a comparison of the experimental data
with the modelling calculations.

To characterize the general shape of the electron
velocity distribution, we have used a 'three-temperature
distribution'. In this model, the tail part of the distribu-
tion is assumed to have Gaussian shape with a perpen-
dicular temperature $T_\perp$ and a forward parallel
temperature $T_{\parallel F}$, as well as a backward parallel
temperature $T_{\parallel B}$. The terms 'forward' and 'backward'
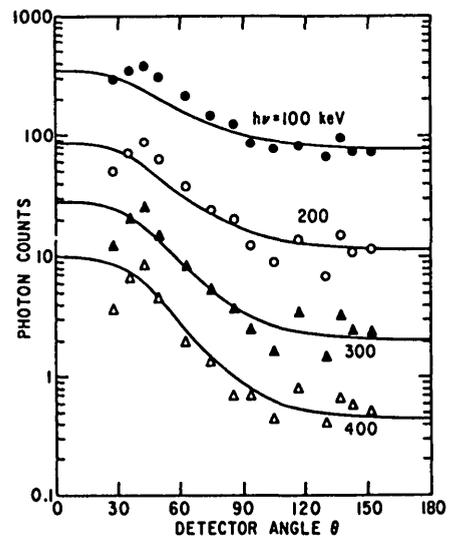
FIG.11. Angular dependence of X-ray emission at photon
energies hν = 100 keV, 200 keV, 300 keV, and 400 keV. Data
points are extracted from Fig.9 by applying geometry correction
factor CF. Solid lines represent bremsstrahlung calculation for
a 'three-temperature' distribution with parameters: forward
temperature $T_{\parallel F}$ = 750 keV, perpendicular temperature
$T_\perp$ = 150 keV, backward temperature $T_{\parallel B}$ = 150 keV, maximum
electron energy E^* = 600 keV. Shape of distribution function is
illustrated in Fig.12.
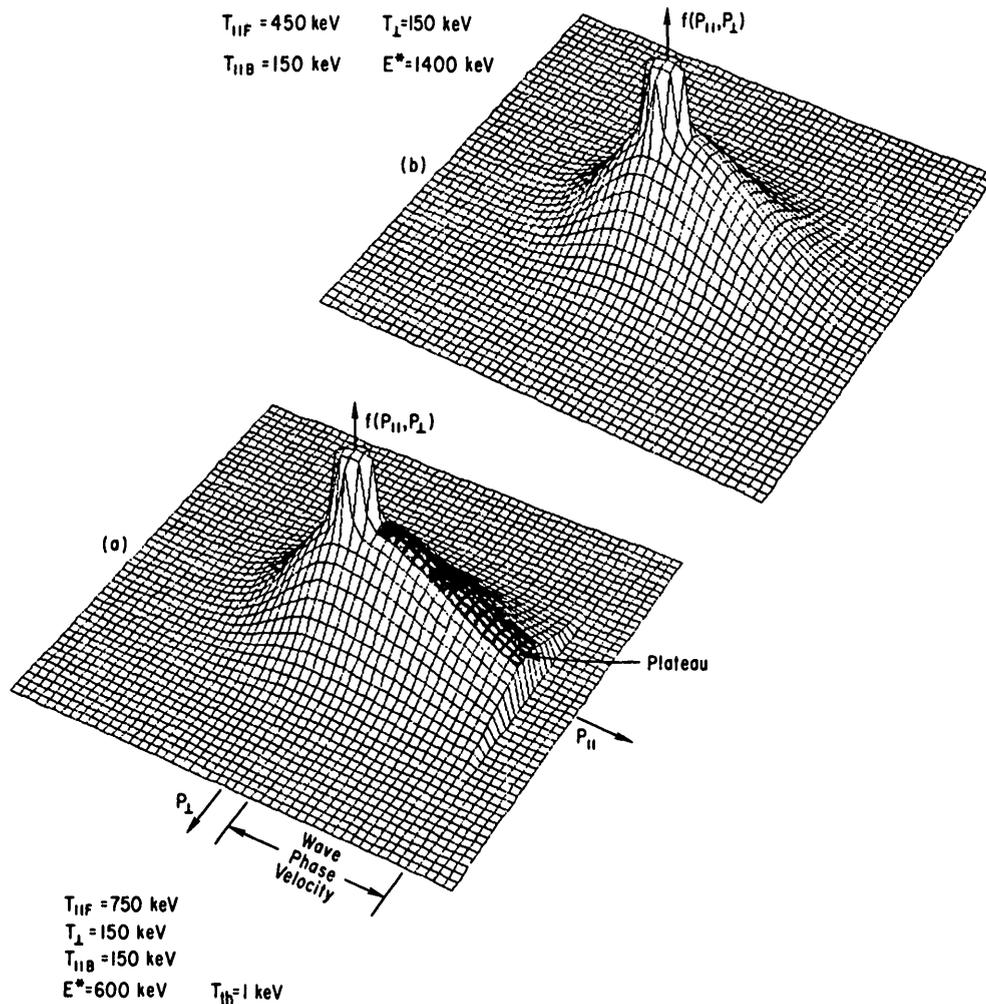
FIG.12. Two distribution functions fitting tangential scan discussed in Section 3. Plateau, thought to be created by Landau damping of lower-hybrid waves, is indicated by shading in (b). Height of distribution function is plotted on linear scale.

refer to the direction of propagation of the lower-hybrid waves. The terms 'parallel' and 'perpendicular' refer to the direction relative to the magnetic field. The ratio of backward going to forward going particles can be varied by changing the backward fraction f_B. The model also uses a cut-off energy E^*, i.e. it is assumed that there are no electrons with energy larger than E^*. The best fit of this model distribution (assumed to be homogeneous in space) is represented in Fig.11 by the solid lines, and was obtained for the following set of parameters: $T_{\|F} = 750$ keV, $E^* = 600$ keV, $T_\perp = 150$ keV, $T_{\|B} = 150$ keV. The parameters of the fit are not determined in a unique fashion; for instance, a fit almost as good as the one shown in Fig.11 is obtained by simultaneously increasing E^* and decreasing $T_{\|F}$, i.e., for the parameter set $T_{\|F} = 450$ keV, $E^* = 1400$ keV, $T_{\|B} = 150$ keV,

$T_\perp = 150$ keV. Two-dimensional graphs of the electron distribution functions corresponding to the two parameter sets are shown in Figs 12a and b. Comparable uncertainties are associated also with the other parameters. For example, the parallel temperature in the backward direction, $T_{\|B}$, can be increased somewhat if the total number of electrons in the backward direction is decreased. Basically, it seems that the total number of particles going either in the forward or in the backward direction, as well as their overall energy, is determined reasonably well. On the other hand, the slope of the distribution function is determined with much less accuracy. This is not meant to say that quantities like the slope of the plateau cannot be measured, in principle, with the bremsstrahlung method. By extending the measurement beyond 500 keV, for example, it should be possible to make a clear distinction
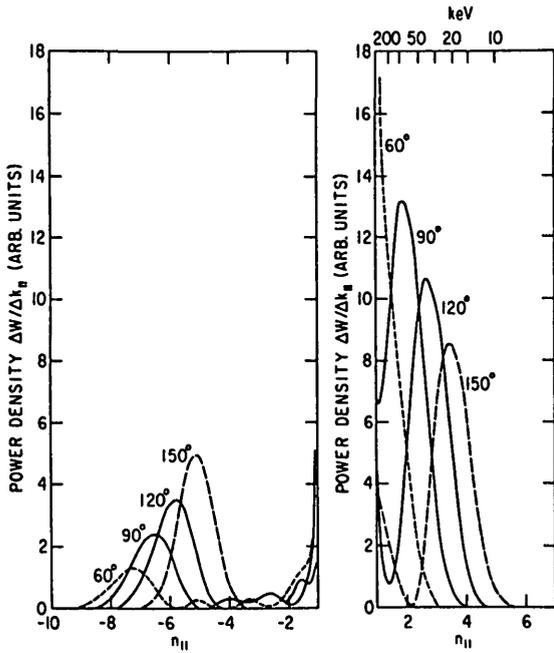
FIG.13. Launched $n_\parallel = c\,k_\parallel/\omega$ spectrum according to Brambilla theory [8] produced by six-element waveguide grill of the 800 MHz lower-hybrid antenna on PLT in the backward and forward directions. Parameter of curves is phasing of wave-guides. Energy of electrons resonating with wave of given $n_\parallel$ is indicated in top right corner.

between the two different distributions shown in Figs 12a and b. The accuracy with which the fitting parameters can be extracted from the bremsstrahlung data is discussed in detail in the accompanying paper [2].

Landau damping of a wave causes a flattening of the velocity distribution function at the phase velocity of the wave. For a continuous wave spectrum, the velocity distribution is flattened over a whole range of velocities, and a plateau is formed as predicted by Karney and Fisch [7] for the lower-hybrid current drive. The distribution function inferred from the measurement has also a plateau, as indicated in Fig.12a. According to Karney and Fisch, the extent of the plateau should depend on the range of the wave spectrum. The RF power spectrum predicted by Brambilla theory [8] for the 800 MHz grill of PLT is shown in Fig.13 for a variety of phasings between neighbouring waveguides. These curves represent the wave spectrum right in front of the lower-hybrid grill. Ray-tracing codes [9] using linear theory predict spectra in the central plasma region for the first pass that are similar to the one shown in Fig.13, but are slightly upshifted in $n_\parallel$. The Landau-damping absorption of the waves as a function of minor radius depends sensitively on the slope of the

energetic electron tail and is not very quantitatively known at present. According to Fig.13, the RF power spectrum for 90° phasing of the waves couples to electrons which have parallel energies ranging from very high energies down to approximately 30 keV. For electron energies lower than 30 keV, there is very little power in the Brambilla spectrum, whereas quasi-linear theory of current drive requires that there should be waves which pull the thermal particles into the tail. According to the PHA X-ray spectrum shown in the inset of Fig.10, the transition from the thermal part of the spectrum to the suprathermal part occurs at about 8 keV in the centre of the plasma, i.e. there exists a spectral gap that extends from 8 keV to 30 keV. The gap in the $n_\parallel$ spectrum is thought at present to be filled by secondary high-$n_\parallel$ waves. There are five proposed mechanisms for producing high-$n_\parallel$ waves from the low-$n_\parallel$ lower-hybrid waves: (1) There is the Bonoli-Ott mechanism [10], in which lower-hybrid waves are scattered by plasma-density fluctuations near the plasma surface. (2) There is the possibility for upshift of $n_\parallel$ after reflection of waves at the plasma surface after one or more passes through the plasma [10, 11]. (3) There is the process proposed by Liu and co-workers [12], in which high-phase-velocity waves excite slower plasma waves via the anomalous Doppler effect. (4) Another possibility is parametric decay [15]. (5) Finally, Succi et al. [16] argue that a small amount (about 4%) of RF power in the range of $n_\parallel$ for filling the gap might exist, because of the non-ideal nature of the experimental spectrum and that this power is sufficient to close the gap. Any one of these processes might be responsible for filling the gap in the RF spectrum at low energies. At the present moment, process (2) is favoured because it does not require any anomalous mechanisms and because it has been shown in modelling calculations to be sufficiently effective in filling the gap in the RF spectrum. The high-phase-velocity limit of the RF power spectrum inside the plasma is determined by wave accessibility considerations. Using a formula from Ref.[14] for the minimum of the refractive index $n_{\parallel a}$ in the central plasma region,

$$n_{\parallel a}^2 = 1 + 2\left(\frac{\omega_{pe}}{\omega_{ce}}\right)^2 - \left(\frac{\omega_{pi}}{\omega}\right)^2$$

$$+ 2\left(\frac{\omega_{pe}}{\omega_{ce}}\right)\left[1 + \left(\frac{\omega_{pe}}{\omega_{ce}}\right)^2 - \left(\frac{\omega_{pi}}{\omega}\right)^2\right]^{1/2}$$

we obtain for our discharge a value $n_{\parallel a} \cong 1.2$. The corresponding electron energy is approximately 400 keV. Brambilla theory predicts that there exist

waves which propagate in the backward as well as in the forward direction. These waves might be responsible for the backward X-ray emission. The measured backward temperature $(T_{\parallel B} = 150 \text{ keV})$ is much lower than the forward temperature, and this feature seems to be qualitatively in agreement with the theoretical predictions. Quantitatively there are discrepancies. According to Fig.13, the main peak of the backward RF power spectrum stretches out to a value of $n_{\parallel} \approx 5$, which corresponds to a maximum electron energy of 10 or 15 keV, much less than the observed energies. In addition, the backward waves may be damped and absorbed before they reach the plasma centre. As in the case of the previously discussed gap in the forward power spectrum, scattering of the waves or reflection after one pass through the plasma can be invoked in order to explain this discrepancy. On the other hand, Fokker-Planck calculations by Karney have shown that a very weak spectrum in the backward direction can produce a sizable backward tail. Perhaps the small residue of power in the region $-2 < n_{\parallel} < -1$ is sufficient, especially since Brambilla theory assumes an idealized grill. To understand these features quantitatively, measurements of the wave spectrum in the plasma centre have to be performed.

A comparison was also made of the measured distribution function with the predictions of Karney-Fisch theory [7]. The details of this comparison are presented in the accompanying paper [2], and we quote here only the main result. The θ-dependence of the X-ray emission in the forward direction seems to be consistent with Karney-Fisch theory, which is based on classical Coulomb scattering of the energetic electrons. There are, however, many parameters like Z_{eff} or the limits of the RF spectrum which have to be adjusted in order to provide a reasonable fit, so that the presence of anomalous processes cannot be ruled out.

There is one feature of the data that is in disagreement with the theoretical curves — the so called 'hump'. The corrected data in Fig.11, and even the raw data of Fig.9, show that the X-ray emission becomes smaller as the angle θ decreases from 45° to 28°. The decrease is more pronounced at higher photon energies. Since this feature has been observed not only in this but also in other discharges, it is believed to be a real effect and not an accidental effect caused, for example, by the non-reproducibility of discharges or by wall radiation. Modelling of the data, which is discussed extensively in the accompanying paper [2], showed that the hump is not to be interpreted as evidence that the energetic electrons have orbits with a pitch angle of 45°. Modelling indicated, on the other hand, that a ring of

highly energetic electrons in the outer plasma regions could account quantitatively for the features of the 'hump'. According to this interpretation, high-energy electrons circling around the torus on magnetic surfaces with minor radius of 20 to 40 cm would see the detector with an effective emission angle $\theta = 0°$ and would cause a strong peaking of the emission at a nominal detector angle of $\theta = 45°$. The radial profile measurement with the PHA system would not detect the presence of very-high-energy electrons because the Si (Li) detector measures only X-rays with energy smaller than 25 keV. In the next section, we will discuss radial profile measurements with a 3 in. × 3 in. NaI detector, which were performed to investigate the hump.

4. RADIAL PROFILES OF THE HARD X-RAY EMISSION FOR DIFFERENT PHOTON ENERGIES

To obtain evidence on the presence of an outer energetic electron ring during lower-hybrid current drive, we have measured the hard-X-ray spectrum as a
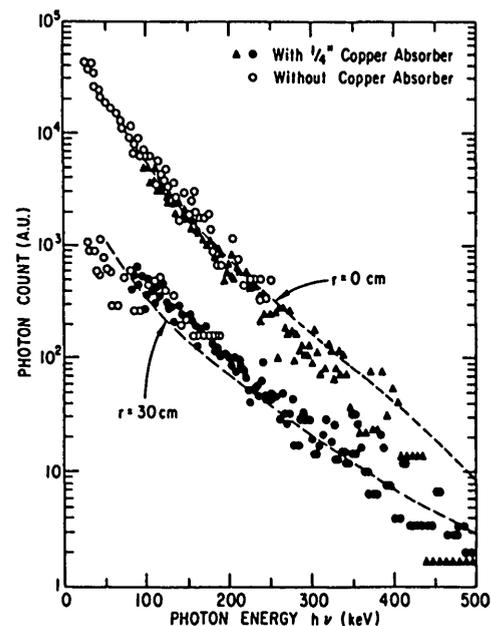
FIG.14. Hard-X-ray spectra measured at minor radii of $r = 0$ and $r = 30$ cm during lower-hybrid current-drive discharge with $\bar{n}_e = 4 \times 10^{12} \text{cm}^{-3}$. Spectrum from plasma centre is much steeper. Dashed line is for inhomogeneous distribution with parameters: in range $0 < r < 20$ cm, parallel forward temperature $T_{\parallel F} = 750 \text{ keV}$, maximum electron energy $E^* = 425 \text{ keV}$, perpendicular temperature $T_{\perp} = 150 \text{ keV}$, parallel backward temperature $T_{\parallel B} = 150 \text{ keV}$, backward fraction $f_B = 1$; in range $20 < r < 40$ cm, $T_{\parallel F} = 5000 \text{ keV}$, $E^* = 800 \text{ keV}$, $T_{\perp} = 225 \text{ keV}$, $T_{\parallel B} = 225 \text{ keV}$, backward fraction $f_B = 0.8$.
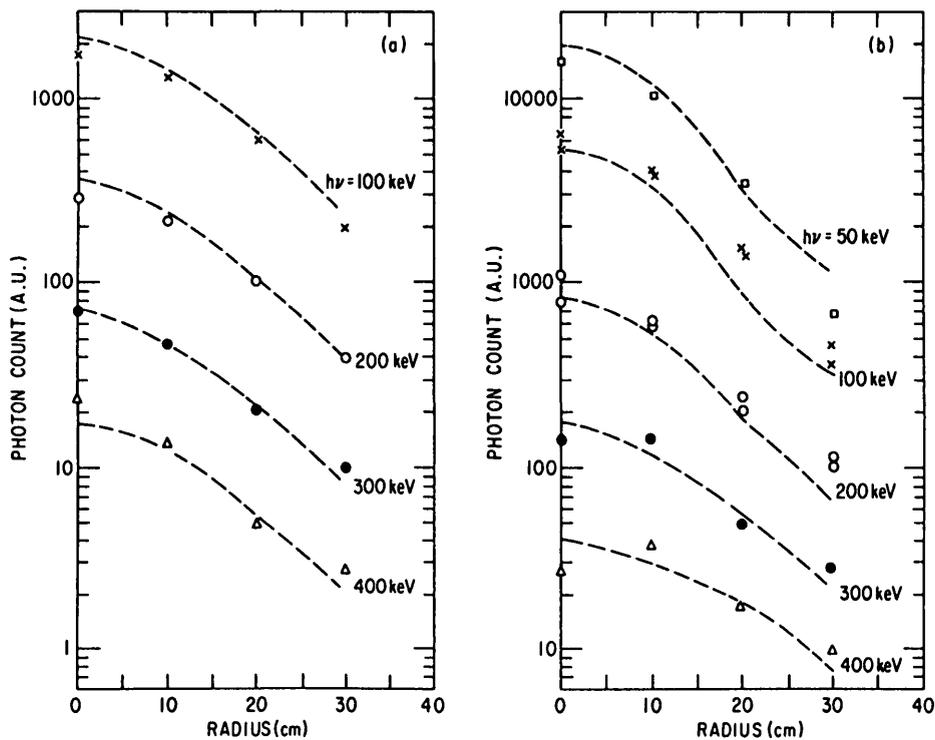
FIG.15. Radial profiles of hard-X-ray emission for various photon energies. Data in (b) indicate
that distribution becomes increasingly more energetic with radius. Data and fit are the same as in
Fig.14. Data in (a) have been measured at lower plasma density $(\bar{n}_e = 2.5 \times 10^{12} cm^{-3})$. In this case,
profiles for different photon energies have the same shape, i.e. distribution function is identical for
all radii. Parameters for fit in (a) are: forward temperature $T_{\|F} = 750$ keV, maximum electron
energy $E^* = 600$ keV, perpendicular temperature $T_{\perp} = 150$ keV, backward temperature $T_{\|B} = 150$ keV
in whole range of $0 < r < 40$ cm.

function of radius looking perpendicular to the mag-
netic field. For this purpose we have replaced the
silicon detector of the PHA (Fig.5) by a 3 in. X 3 in.
sodium-iodide (NaI) detector and performed radial
scans. Unfortunately, these measurements were done
after the tangential detector was removed from the
tokamak, so a direct comparison with tangential scans
for the same discharge was not possible. This is
important because the results with the 3 in. X 3 in. NaI
detector seem to vary when plasma parameters are
changed. Typical data in support of the hot 'electron
ring' hypothesis are shown in Figs 14 and 15b. Data
without the ring are shown in Fig.15a. In Fig.14, a
comparison is shown between a hard-X-ray spectrum
from the central (r = 0) and from the outer (r = 30 cm)
region of the plasma column. The data points represent
measurements taken with (dots and triangles) or without
(open circles) a 1/4 in. copper absorber inserted into
the X-ray line of sight. The function of the copper
absorber was to screen out low-energy photons so that

the high-energy X-rays could be lifted out of the general
hard-X-ray background without increasing the count rate.
The solid lines are generated from the modelling calcu-
lations and represent the X-ray emission of an inhomo-
geneous electron distribution with the following
parameters: in the range $0 < r < 20$ cm, forward
temperature $T_{\|F} = 750$ keV, maximum electron energy
$E^* = 425$ keV, perpendicular temperature $T_{\perp} = 150$ keV,
and parallel backward temperature $T_{\|B} = 150$ keV; in
the range $20 < r < 40$ cm, $T_{\|F} = 5000$ keV, $E^* = 800$ keV,
$T_{\perp} = 150$ keV, $T_{\|B} = 150$ keV. It was assumed that the
radial profile is approximately the same as the one in
Fig.10, i.e. the distribution function in the outer region
was only about 10% of the distribution function in the
central region. The X-ray spectrum from the central
region has a steeper slope than the spectrum from the
outer region, and the measured data are in reasonable
agreement with the theoretical predictions. There
exists then some evidence that the 'hump' is due to the
presence of higher-energy electrons on the outside of
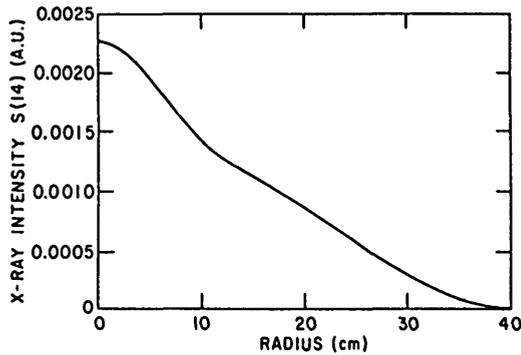
FIG.16. Radial profile of X-ray emission at photon energy of 14 keV for low-magnetic-field discharge (toroidal magnetic field $B_T = 20$ kG, plasma current $I_p = 270$ kA).

the torus. On the other hand, when the LH current drive operated at slightly lower plasma densities, this feature disappeared. This is illustrated in Figs 15a and b, where the X-ray emission for various photon energies is plotted versus radius. Figure 15b represents the same data as Fig.14. The radial profile of 50 keV X-ray emission is much more peaked than the 300 keV or 400 keV X-ray emission. In Fig.15a, on the other hand, the radial profiles for the low-energy X-ray emission have about the same shape as the high-energy X-ray emission, and a simple homogeneous distribution function provides a perfect fit. These data suggest then that the hump is caused by the fact that the electrons on the outside of the torus are more energetic. The low-density data indicate furthermore that the hump is not a general feature of lower-hybrid current drive discharges.

5. VARIATION OF THE DISTRIBUTION FUNCTION WITH DISCHARGE CONDITIONS

In this section, we present data that show how the electron distribution behaves as plasma parameters are varied. These results should be considered incomplete because our experiment was operational on the machine only for a very short time period. As a consequence, we show here the limited available data that we obtained rather than results from a careful systematic survey. The data consist of (a) a tangential scan at low toroidal magnetic field, (b) an investigation of the effect of different phasings of the waveguide grill on the distribution function, and (c) a comparison of a runaway discharge with lower-hybrid current drive.

(a) Tangential scan at a lower toroidal magnetic field: For lower magnetic field, or more precisely for

smaller safety factor q, the hard-X-ray emission has a much wider profile, as shown in Fig.16. With the wider profile, the interpretation of the tangential scan is not so sensitive to small errors in the profile measurement. The unfolded data from the low-field scan are shown in Fig.17b. The best fit from the modelling of the distribution function is shown in Fig.17a, and the resulting bremsstrahlung is represented by the solid lines in Fig.17b. The step in the distribution function at $p_\parallel = 0$ is caused by setting the backward function $f_B < 1$. The step is, of course, unphysical and should be smoothed out. Apart from a slightly higher backward temperature $T_{\parallel B}$, the distribution function seems identical with the high-field result. On the other hand, the current drive efficiency for the 800 MHz current drive is, in general, considerably reduced at low
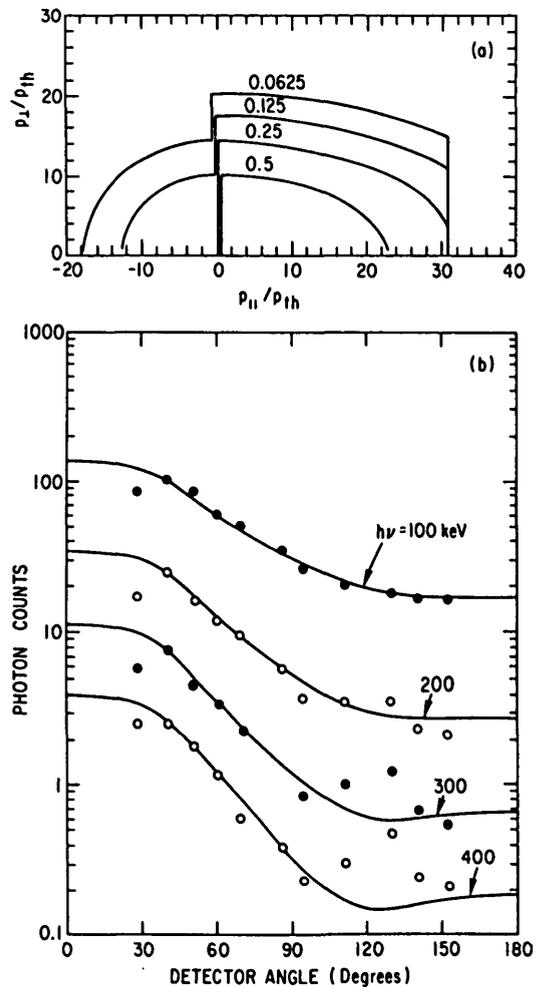
FIG.17. Tangential scan of hard-X-ray emission for low toroidal magnetic field. Parameters for fit are: forward temperature $T_{\parallel F} = 750$ keV, perpendicular temperature $T_\perp = 150$ keV, backward temperature $T_{\parallel B} = 225$ keV, maximum electron energy $E^* = 600$ keV, backward fraction $f_B = 0.25$.
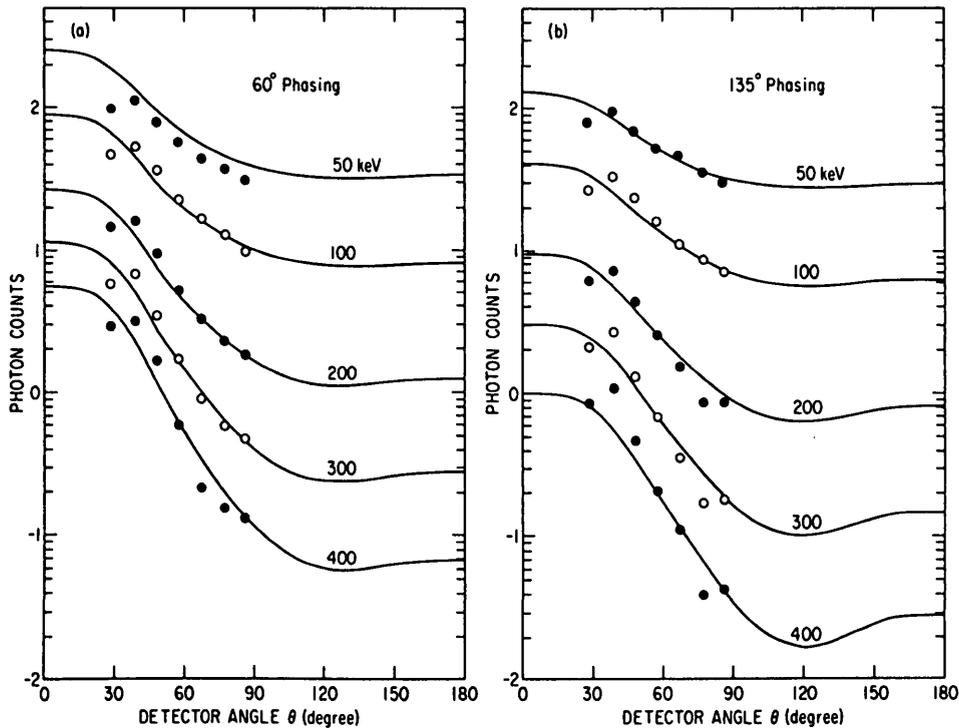
FIG.18. Tangential scans for (a) 60° phasing and for (b) 135° phasing of waveguide grill.
Parameters for bremsstrahlung fit: for 60° phasing forward temperature $T_{\|F} = 1200$ keV,
maximum electron energy $E^* = 1000$ keV, perpendicular temperature $T_\perp = 125$ keV, backward
temperature $T_{\|B} = 175$ keV, backward fraction $f_B = 0.8$; for 135° phasing $T_{\|F} = 750$ keV,
$E^* = 600$ keV, $T_\perp = 90$ keV, $T_{\|B} = 150$ keV, $f_B = 0.8$. Line average density was $4 \times 10^{12} cm^{-3}$
for (a) and $3.75 \times 10^{12} cm^{-3}$ for (b). RF power was 100 kW for (a) and 370 kW for (b).

magnetic fields. There are no indications in the X-ray spectra why the efficiency is smaller at low fields.

(b) Tangential scans for different phasing of the waveguide grill: the angular distribution of the X-ray emission for 60° and for 135° phasing is shown in Fig.18a and b, respectively. Because of the limited available time, the scans were performed only in the forward direction. To hold the current flat, considerably more RF power was applied in the case of the 135° phasing (370 kW versus 100 kW). To carry out modelling calculations for these incomplete scans, it was assumed that the backward X-ray emission is constant between $90° < \theta < 180°$. The solid lines represent the best fit of the modelling with the three-temperature code. For the 60° phasing we obtain the following parameters: forward temperature $T_{\|F} = 1200$ keV, maximum energy $E^* = 1000$ keV, perpendicular temperature $T_\perp = 125$ keV, backward temperature $T_{\|B} = 175$ keV, backward fraction $f_B = 0.8$. The corresponding parameters for the 135° phasing were $T_{\|F} = 750$ keV, $E^* = 600$ keV, $T_\perp = 90$ keV,

$T_{\|B} = 150$ keV, with a backward fraction $f_B = 0.8$. As reported previously [5a], the X-ray spectra emitted in the perpendicular direction are much steeper for the 135° phasing. These scans reveal also that the forward spectra are much steeper. Such behaviour is expected from theory, because the 135° phasing of the grill gives rise to a much slower wave spectrum (Fig.13). However, the quantitative modelling reveals severe discrepancies. The measured spectra indicate that the maximum forward energy is reduced from $E^* = 1000$ keV for 60° phasing to $E^* = 600$ keV for 135° phasing. This reduction is not as large as expected. The theoretically calculated $n_\|$ power spectrum for 135° peaks around 30 keV and becomes quite small around 100 keV. To reconcile this discrepancy between theory and experiment, we have to postulate conversion of slow into fast waves for the 135° phasing. The mechanisms responsible for this conversion are probably the same processes that have been invoked to close the gap in the case of 60° and 90° phasing as discussed in Section 3. Since secondary waves may be
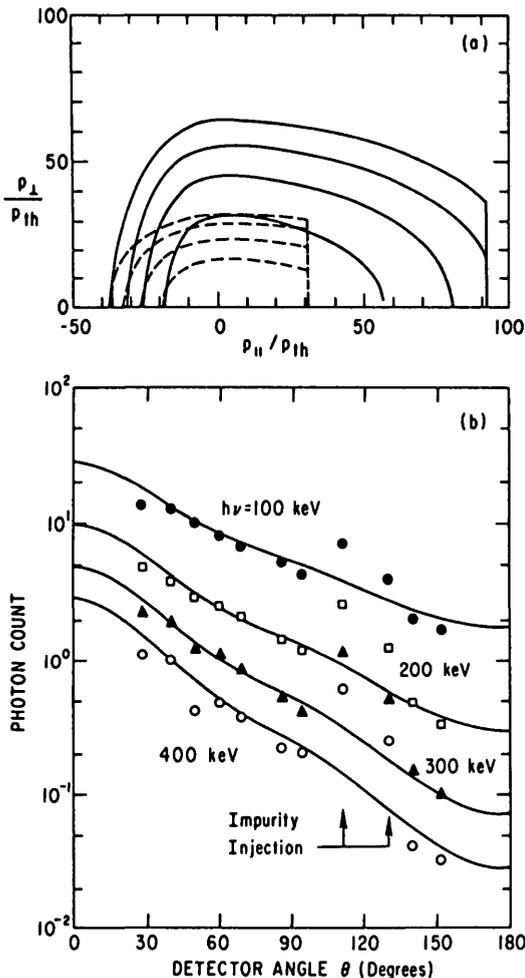
FIG.19. Tangential scan of runaway discharge. Parameters for bremsstrahlung fit of data: parallel forward temperature $T_{\|F} = 1400$ keV, maximum energy $E^* = 2500$ keV, perpendicular energy $T_\perp = 450$ keV, backward temperature $T_{\|B} = 140$ keV, backward fraction $f_B = 1$. For comparison, electron distribution during lower-hybrid current drive is indicated by dashed lines in (a). Each contour represents a factor of 10.

responsible for the current drive at 135° phasing, and since there seems to be less power in the secondary wave spectrum, it seems reasonable to look at the X-ray emission at 30 keV, where the $n_\|$ spectrum peaks, and investigate whether there is enhanced emission in that region. Experimentally, it was observed that the emission at $h\nu = 50$ keV or $h\nu = 25$ keV is larger for 135° than for 60°. However, the low-energy emission was weaker than predicted by modelling for both cases. Since no records were kept on the low-energy threshold setting of the discriminators of the X-ray amplifiers, it is not clear whether the X-ray data are reliable at these low energies. Actually, the need to postulate secondary low-$n_\|$ waves

for 135° phasing does not seem quite as urgent as the need to postulate secondary high-$n_\|$ for the gap of the 60° or 90° phasing. Most of the collisional losses occur for low-energy electrons, and there is a small residue of power left in the range $1 < n_\| < 2$ for 135° phasing, which, for a launching antenna less perfect than Brambilla theory assumes, might be sufficient to drive the current. The real puzzle is why the 60° phasing is so much more efficient than the 135° phasing in spite of the large gap in the launched spectra.

(c) Comparison of the electron distribution during lower-hybrid current drive with an electron-runaway distribution: Actually, a special tangential scan for an electron runaway discharge was not performed. However, after termination of the RF power in a typical current drive discharge, the discharge goes on for several hundred more milliseconds with the driving voltage being supplied by the $-LdI/dt$ term from the decay of the plasma current. The hard-X-ray emission tends to decrease in intensity during this time and simultaneously to become much more energetic. The decay time of the hard-X-ray amplitude amounts to several 100 ms. The hard-X-ray spectra measured during this phase are very similar to spectra from runaway discharges. A tangential scan taken in the time interval 250 to 300 ms after turning off the RF is shown in Fig.19b. The measured X-ray emission looks much more peaked in the forward direction than for comparable current drive discharges. The data exhibit no hump! (The increased X-ray emission at $\theta = 110°$ and $\theta = 130°$ is due to selenium impurity injection with laser blow-off.) The following parameters were used in the modelling to calculate the solid curves: forward temperature $T_{\|F} = 1400$ keV, maximum electron energy $E^* = 2500$ keV, perpendicular energy $T_\perp = 450$ keV, backward temperature $T_{\|B} = 140$ keV. In Fig.19a this runaway electron distribution is compared with the current drive distribution from Section 2. Runaway discharges tend to exhibit relaxation oscillations, which may be the reason why the perpendicular temperature $T_\perp$ is so high. This figure underscores the important difference in the behaviour of runaway and LH-current-drive discharges. The electron distribution in a current drive discharge is only mildly relativistic, and most tail electrons have an energy of only a few hundred keV. On the other hand, in a runaway discharge the electron energy seems to extend well beyond 1 MeV. Our measurements, which extend only to $h\nu = 400$ keV, do not tell us very accurately what exact shape the distribution function has in the MeV range.

6. CONCLUSIONS

Measurements of the bremsstrahlung emission as a function of the angle between the magnetic field and the direction of emission have allowed us to determine the velocity distribution function during lower-hybrid current drive. The following summary lists our most important findings:

1. The bremsstrahlung emission intensity in the forward direction is about one order of magnitude larger than in the backward direction. This shows that most of the tail electrons go in the forward direction. There is a small backward tail. It has a much smaller energy content than the forward tail.

2. Modelling of the data shows that the electron tail represents a relatively flat distribution that extends out to several hundred keV energy and carries the total current during lower-hybrid current drive. A Z_{eff} of 4, which is necessary to make the bremsstrahlung emission from the model agree with the hard-X-ray data, is consistent with soft-X-ray PHA data. The tail does not seem to extend very much beyond 1 MeV during LH current drive.

3. The tail of the distribution is interpreted as the quasi-linear plateau created by Landau damping of the lower-hybrid waves. The shape of the $n_{\parallel}$ wave spectrum in the plasma can then be inferred from the measured distribution function. A process that shifts part of the launched $n_{\parallel}$ spectrum upward has to be invoked to explain the 'gap' problem for $60°$ and $90°$ phasing. A similar process may shift the $n_{\parallel}$ spectrum down for $135°$ phasing and for the backward spectrum. The unexpectedly more energetic X-ray spectra in the two latter cases can also possibly be explained by the small residual power for $|n_{\parallel}| < 2$.

4. The perpendicular slope of the distribution function is not inconsistent with collisional relaxation of the distribution function, as proposed by the Karney-Fisch theory. In view of the small-scale noise on the traces of the $2\omega_{ce}$ emission, this point is not emphasized since the noise could be an indication of some non-collisional process.

5. A comparison of the electron distribution during LH current drive with a runaway distribution shows that the lower-hybrid electrons are much less energetic than runaway electrons.

REFERENCES

[1] BERNABEI, S., DAUGHNEY, C., EFTHIMION, P., HOOKE, W., HOSEA, J., et al., Phys. Rev. Lett. **49** (1982) 1255.

[2] STEVENS, J., VON GOELER, S., BERNABEI, S., BITTER, M., CHU, T.K., et al., accompanying paper, this issue, p.1529.

[3] VON GOELER, S., STEVENS, J., KARNEY, C., BERNABEI, S., BITTER, M., et al., in Radio Frequency Plasma Heating (Proc. 5th Top. Conf. Madison, 1983) 96–108.

[4] SHOHET, J.L., Phys. Fluids **11** (1968) 1065; ENGLAND, A., HASTE, G., Phys. Rev. **A7** (1973) 383; Phys. Rev. **A8** (1973) 1475.

[5] a) VON GOELER, S., STODIEK, W., in Controlled Fusion and Plasma Physics (Proc. 5th Europ. Conf. Grenoble, 1972), Vol.1 (1972) 2; b) VON GOELER, S., STEVENS, J., STODIEK, W., BERNABEI, S., BITTER, M., et al., in Diagnostics for Fusion Reactor Conditions (Proc. Course Varenna, Italy), EUR 8351-IEN, Vol.1 (1982) 87.

[6] SESNIC, S., TENNEY, F., BITTER, M., HILL, K., VON GOELER, S., Rev. Sci. Instrum. **56** (1985) 1160.

[7] KARNEY, C., FISCH, N., Phys. Fluids **22** (1979) 1817.

[8] BRAMBILLA, M., Nucl. Fusion **16** (1976) 47.

[9] IGNAT, D., Phys. Fluids **24** (1981) 1110.

[10] BONOLI, P., OTT, E., Phys. Fluids **25** (1982) 359.

[11] VALEO, E., EDER, D. (private communication).

[12] LIU, C.S., CHAN, V., BHADRA, D., HARVEY, R., Phys. Rev. Lett. **48** (1982) 1479.

[13] TROYON, F., PERKINS, F.W., in Radio Frequency Plasma Heating (Proc. 2nd Top. Conf. Lubbock, 1974) (1974) Paper B4-1.

[14] BERS, A., in Radio Frequency Plasma Heating (Proc. 3rd Top. Conf. Pasadena, 1978) (1978) Paper A1-1.

[15] OHKUBO, K., TOI, K., KAWAHATA, K., KAWASUMI, Y., MATSUMOTO, K., et al., Nucl. Fusion **25** (1985) 732.

[16] SUCCI, S., APPERT, K., MOREAU, D., VACLAVIK, J., in Plasma Physics and Controlled Nuclear Fusion Research (Proc. 10th Int. Conf. London, 1984), Vol.1, IAEA, Vienna (1985) 549.